Surface imaging using holographic optical tweezers

2011 Nanotechnology 22 285503

(http://iopscience.iop.org/0957-4484/22/28/285503)

Nanotechnology **22** (2011) 285503 (7pp) doi:10.1088/0957-4484/22/28/285503

Surface imaging using holographic optical tweezers

D B Phillips[1], J A Grieve[1], S N Olof[1], S J Kocher[1], R Bowman[2], M J Padgett[2], M J Miles[1] and D M Carberry[1]

[1] H H Wills Physics Laboratory, University of Bristol, Tyndall Avenue, Clifton, Bristol BS8 1TL, UK
[2] SUPA, Department of Physics and Astronomy, University of Glasgow, Glasgow G12 8QQ, UK

E-mail: david.carberry@bristol.ac.uk

Received 4 March 2011, in final form 19 April 2011
Published 7 June 2011
Online at stacks.iop.org/Nano/22/285503

Abstract

We present an imaging technique using an optically trapped cigar-shaped probe controlled using holographic optical tweezers. The probe is raster scanned over a surface, allowing an image to be taken in a manner analogous to scanning probe microscopy (SPM), with automatic closed loop feedback control provided by analysis of the probe position recorded using a high speed CMOS camera. The probe is held using two optical traps centred at least 10 μm from the ends, minimizing laser illumination of the tip, so reducing the chance of optical damage to delicate samples. The technique imparts less force on samples than contact SPM techniques, and allows highly curved and strongly scattering samples to be imaged, which present difficulties for imaging using photonic force microscopy. To calibrate our technique, we first image a known sample—the interface between two 8 μm polystyrene beads. We then demonstrate the advantages of this technique by imaging the surface of the soft alga *Pseudopediastrum*. The scattering force of our laser applied directly onto this sample is enough to remove it from the surface, but we can use our technique to image the algal surface with minimal disruption while it is alive, not adhered and in physiological conditions. The resolution is currently equivalent to confocal microscopy, but as our technique is not diffraction limited, there is scope for significant improvement by reducing the tip diameter and limiting the thermal motion of the probe.

(Some figures in this article are in colour only in the electronic version)

1. Introduction

Numerous fields ranging from cellular biology through to device fabrication use scanning probe microscopy (SPM) to determine surface topography [1–3]. The broad applicability of the technique stems from its ability to map out the location of nanoscale features, such as surface defects in semiconductors [4] or receptor sites on cell membranes under physiological conditions [5–7]. Modification of probe surface chemistry has enabled the interactions between various functionalized surfaces to be investigated [8] and has spawned techniques such as force–volume interaction mapping. SPM instrumentation research is mainly aimed at increasing the rates at which surface images are obtained [9, 10], and in lowering the interaction forces [11]. Optical tweezers [12] and photonic force microscopy (PFM) [13] have also been used to identify surfaces within a sample. Using PFM, probe particles have been held in the optical trap and their inherent Brownian motion used to map the cavities in which they are located [14]. Atomic force microscopy (AFM) 'contact-mode' functions have been replicated within optical tweezers by translating a trapped probe along a surface [15, 16], and an optically trapped scanning near-field optical microscope (OT-SNOM) has also been demonstrated [17].

Each of these techniques (SPM, PFM) has its own strengths, but is also subject to its own set of constraints. SPMs can record pixels at MHz rates, are able to use tips which can taper to a single atom, and they are able to tune the residual Brownian motion to amplitudes of less than 1 nm. However, they require relatively flat samples and operate in an orientation that is perpendicular to the surface. Contact and tapping mode AFMs also exert relatively large forces

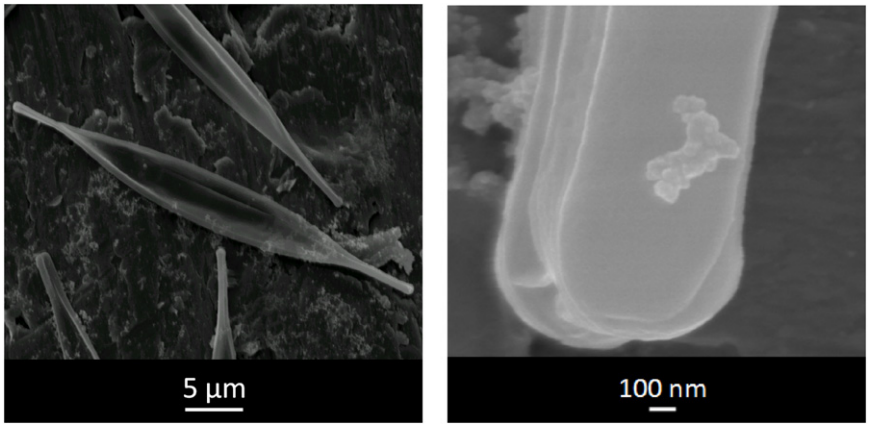

(a) (b)

Figure 1. (a) An SEM image showing typical diatoms used in the experiments. (b) An SEM image of the tip of a single diatom. As can be seen the tip has a radius of curvature of approximately 350 nm. This is within the natural tip variance of the diatoms: 200–500 nm.

on samples [18], of the order of hundreds of piconewtons, which can damage sensitive biological specimens. Optical tweezers and PFMs are sensitive to very low forces, typically in the range of tens of femtonewtons. This force sensitivity comes at the price of lower positional resolution, which is limited by Brownian motion and the size of the probe particle. Additionally, PFMs exert high laser intensities near the sample and are ineffective in environments where samples are likely to cause beam interference or occlusion.

The aim of this work is to combine the strengths of SPM and optical tweezers to image any surface. Our technique uses a probe held by two optical traps (figure 2) which can be dynamically reconfigured to reorient the probe using holographic beam shaping [19, 20]. This enables the imaging of cells with low elastic moduli, minimizing membrane disruption and allowing the investigation of cells not adhered to a substrate. Using this technique, we can vary the orientation and position of our probe, scan along any path or axis, and remove the probe tip from the laser focus—limiting the laser intensity which is incident on the sample. This technique grants access to samples which are highly curved or have challenging surface geometries in their native environments.

2. Experimental details

2.1. Holographic optical tweezers setup

Our holographic optical tweezers are slightly modified from those reported in [21]. The system consists of an inverted brightfield microscope with a 1.4 NA, 100× objective (Plan-Neofluar, Zeiss), a motorized xy stage (MS-2000, ASI) and a closed loop piezoelectric objective lens positioning system (Piezosystem Jena, Mipos 140 PL). The trapping beam is provided by a Nd:YAG laser (Laser Quantum) emitting up to 3.2 W at 1064 nm. The beam is expanded to fill a spatial light modulator (Hamamatsu, X10468-07), the hologram on which determines the resulting optical trap locations, and imaged onto the back aperture of the objective lens. A polarizing beam splitter is used before the objective to transmit the laser beam while reflecting half of the illumination light onto a Firewire CMOS camera (Prosilica, EC1280). Image analysis and feedback control were implemented in LabVIEW (National Instruments) [22] running on a quad core PC, which also contained the graphics processor (GPU) used for hologram calculation (nVidia, Quadro FX 5600). Further details on hologram generation and use of the GPU can be found in [23].

2.2. Preparation of probes

Probes can take a variety of forms—from the microtools previously reported [24–27] through to microscopic organisms. Here we have elected to use the diatom *Nitzschia acicularis* (Kützing) W Smith as the optically trapped probe as it can be easily trapped and manipulated in 3D. SEM images of typical diatoms are shown in figure 1. The diatoms are stored in diatom medium, which promotes cell division and acts as the trapping medium. The diatom is primarily composed of a large, central cylindrical mass, which tapers to a rounded point between 400 and 1000 nm in diameter. This structure provides several advantages over a pure cylinder: the tapering of the silica shell gives a slender probe with a small contact area which is ideal for probe microscopy, and the larger size of the central cylinder has a higher trapping constant than a microrod of constant width equal to the tip diameter. Optical images show two elliptical structures where light is focused, which are used as the optical trapping locations.

Tracking the two high-intensity elliptical structures using a centre-of-mass algorithm, and utilizing the methods described in [28, 26], enables the translational and rotational motion within the focal plane to be recorded at approximately 250 Hz. Equipartition is then used to calibrate the stiffness of the probe in the trap resulting in $\boldsymbol{\kappa} = (\kappa_z, \kappa_x, \kappa_\theta) = (1.8\times10^{-5}\ \mathrm{N\ m^{-1}}, 5.7\times10^{-5}\ \mathrm{N\ m^{-1}}, 1.6\times10^{-15}\ \mathrm{N\ m\ rad^{-1}})$, where z is parallel to the probe's long axis, x is normal to the probe's long axis and θ is the rotational deviation within the focal plane about the optical stress centre. As position tracking was only possible within the focal plane, we elected to employ an image comparison algorithm to detect probe translations

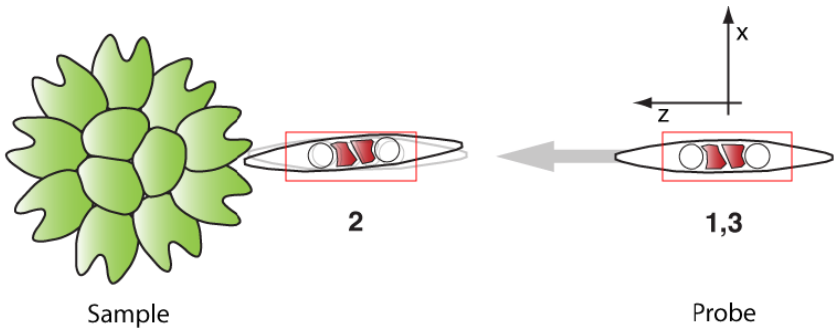

Figure 2. A schematic showing the key points during the imaging of a sample. Dimensions and translations have been exaggerated for clarity. At State 1 the probe is positioned such that there is no physical contact with the sample and the base image is recorded. The probe is advanced in a stepwise manner until it makes contact in State 2, causing the probe to rotate or translate relative to the optical traps. This results in a change in the image comparison routine, allowing the interaction to be detected and the coordinates of the pixel recorded. The probe is moved back to its original configuration, to State 3, and then moved to the next pixel's starting location. These steps are repeated in a raster scan to obtain a whole image.

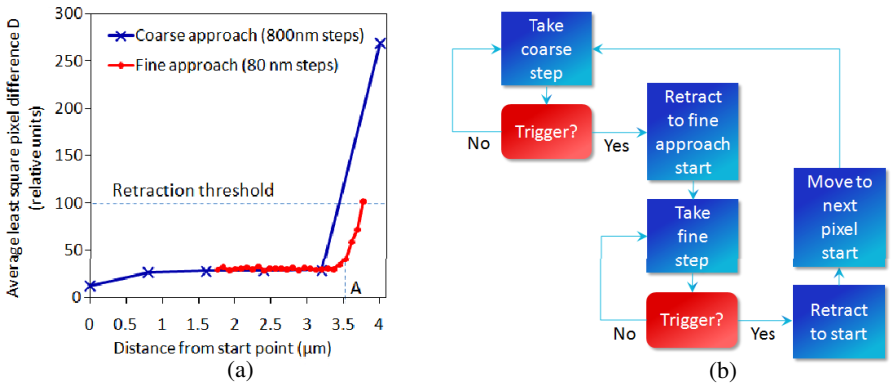

Figure 3. (a) An example of an interaction curve showing coarse and fine approaches to detect contact with the sample. The coarse approach (blue crosses) allows approximate detection of the sample. A coarse withdrawal to the start of the fine approach (red circles) ensues. The fine approach then detects the surface more accurately, resulting in contact at point A. (b) A flow diagram describing the feedback control loop used to detect the height of each pixel in the image.

and rotations in and out of the focal plane. While this does not provide quantitative forces acting on the sample, it does provide an accurate surface profile.

2.3. Imaging methodology

The height z of each pixel in the surface image is obtained in a manner analogous to AFM force–volume mapping. The probe is positioned at the desired (x, y) pixel coordinate such that it is not in contact with the sample, State 1 in figure 2. A region of interest (ROI) is defined (red box in figure 2), and a base image recorded. The positions of the ROI and optical traps are updated to move the probe a step in the z direction towards the sample. Once the probe has moved to its new position another image of the probe is recorded, the stepped image. To reduce the effect of the probe's thermal motion, both the base and stepped images are an average of five consecutively recorded images—a compromise between noise reduction and imaging speed. The average square of the difference D in intensity between the base image and the stepped image is calculated using:

$$D = \frac{\sum_{i,j}(x_{i,j} - \hat{x}_{i,j})^2}{N} \tag{1}$$

where $x_{i,j}$ is the greyscale value of the pixel in row i and column j of the base image, $\hat{x}_{i,j}$ is the same pixel in the stepped image, and N is the total number of pixels in each image. As the ROI is translated the same distance as the traps, provided the probe has not yet contacted the sample, the images will be similar and D will be small. If the probe has made contact with the sample it will translate and/or rotate relative to the optical traps (State 2 in figure 2). The resulting difference in the base image and the stepped image increases the relative magnitude of D. When D exceeds a nominated threshold the probe is defined as in contact with the sample, and retracted. The probe control and image analysis is performed in real time by an automated LabVIEW routine at approximately 30 Hz.

To maximize imaging speed and resolution two interaction curves were recorded for each pixel. A coarse approach was performed with large steps to quickly detect the sample (blue crosses in figure 3(a)). The maximum normal force can be estimated by assuming a full coarse step occurs after contact, resulting in a maximum normal force of 14 pN. When D

exceeded the pre-determined threshold value a two to three step coarse withdrawal occurs. The new probe location is closer to the sample than the original probe's starting position, for example the first red point in figure 3(a). A fine approach is then performed with smaller steps, thereby increasing the z resolution. When D exceeds the threshold value in the fine scan the probe is coarsely withdrawn and moved to the coordinate defining the start of the next pixel. The flowchart in figure 3(b) illustrates this process.

Values of D are recorded for every step during the imaging process, therefore each pixel has an associated coarse and fine interaction curve—akin to AFM force–volume mapping. Sample images are reconstructed from these curves in post-processing, by evaluating the point in the interaction curve at which the image starts to differ significantly from the background noise (point A in figure 3(a)).

The pixel measurement order follows a raster scan pattern. After each pixel is detected and the probe fully retracted, the traps are stepped in the x direction to the adjacent pixel. When a row is completed, the objective lens positioning system is used to step the focal plane to the next row of pixels to be scanned. This simultaneously changes the height of the probe and the focal plane relative to the sample. All scan parameters can be modified by the operator. This imaging method offers the potential to reorient the probe during the imaging from pixel to pixel. For example, the scan path could follow a raster scan that has been mapped onto a cylinder, allowing continuous scanning around a sample, or other arbitrary trajectories.

3. Results and discussion

To characterize the technique, a selection of 8 μm latex spheres were rigidly adhered to a coverslip. The sample was searched until two microspheres were found in contact, and our technique used to image the contact region. Figure 4(a) shows a 3D surface plot of the contact area between the two microspheres. It also indicates the x (lateral) and y (vertical) probe stepsize used to discretely sample the surface, and the fine approach stepsize z towards the surface for each pixel. The colourbar indicates the depth z on the surface plot. The axes show the orientation of the coordinate system used in all subsequent plots. The dark blue base of the surface represents where the probe has continued past the gap between the microspheres undisturbed, and reached a designated zero point. Figure 4(b) demonstrates the experimental configuration with the diatom probe approaching the two latex spheres. The red box around the centre of the probe indicates the border of the region of interest that was maintained around the trap positions as the probe was translated towards the sample.

In a manner analogous to SPM, the number of samples per line and the sampling stepsize may be changed to image different sized areas at varying resolution. This allows the user to zoom in on areas of interest. Figure 5(a) shows a zoomed in image of a similar 8 μm latex sphere interface, where the sampling stepsize has been reduced from 320 to 160 nm. Figure 5(b) shows the linescan from this image around the equator of the microsphere. It demonstrates that the radius of curvature of the diatom tip is approximately 250 nm, within

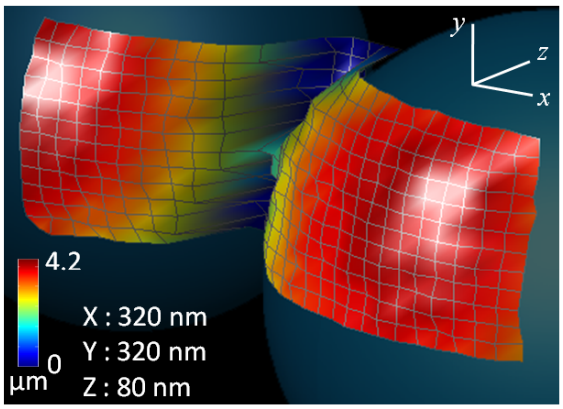

(a)

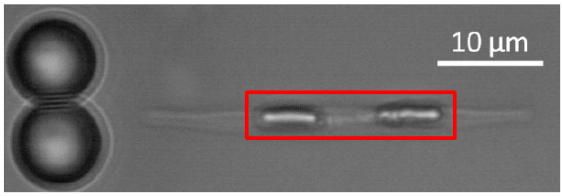

(b)

Figure 4. (a) A 3D surface scan of the interface between two 8 μm latex microspheres. The x (lateral), y (vertical) and z (approach) probe stepsize used to discretely sample the surface are also indicated, along with the coordinate system used. The colourbar indicates the depth z on the surface. Background spheres have been added to the image to indicate the position of the microspheres. (b) An optical image of the experimental configuration, with the diatom probe approaching the microspheres. The red box indicates the region of interest defining the portion of the image used to determine when the probe is in contact with the sample.

the natural variance, and confirms that the microspheres are 8 μm in diameter.

After characterizing the imaging quality using microspheres, a biological sample was imaged. The 3D crown structure and soft cellular walls of the green alga *Pseudopediastrum boryanum* (Turpin) E. Hegewald prevents traditional SPM from being used, and the strongly scattering structure prevents PFM and optical tweezers from imaging the surface. It represents a challenging sample on which to demonstrate our imaging technique. The *Pseudopediastrum* was cultured and stored in 3N-BBM + V (Bolds' basal medium with three-fold nitrogen and vitamins). Samples were prepared by adding an aliquot of diatom and *Pseudopediastrum* medium to a glass chamber. Figure 6 shows an optical image and confocal slice of a typical *Pseudopediastrum* colony.

The probe was first positioned alongside a single *Pseudopediastrum* colony which had settled onto the coverslip, as shown in figure 7(b). As the *Pseudopediastrum* was not adhered to the substrate, it could be easily moved if sufficient laser power was directly applied. Our technique was utilized to obtain images of a single spike in the algal structure (figure 7(a)) and an image of the entire wall of a single *Pseudopediastrum* unit cell (figure 7(c)). For comparison, figure 7(d) shows an image of a similar sample obtained by brightfield confocal microscopy.

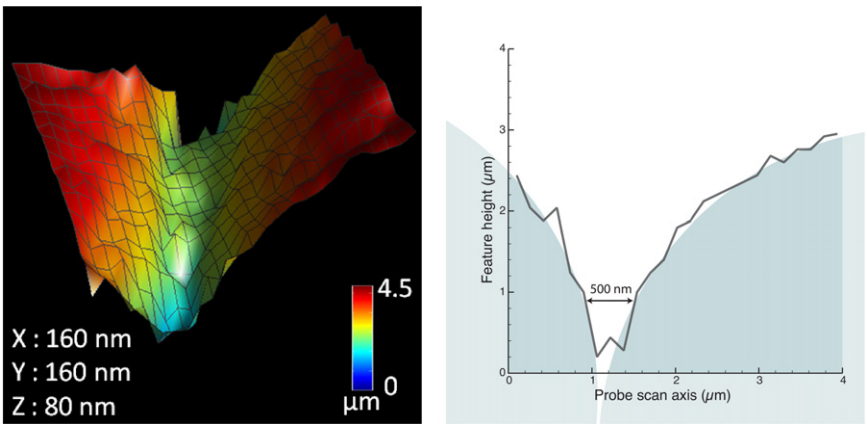

(a) (b)

Figure 5. (a) A higher resolution 3D surface representing the interface of two 8 μm microspheres. (b) A single line scan from (a) through the equator of the two 8 μm microspheres. The measured gap between the spheres is approximately 500 nm, demonstrating that the probe's radius of curvature is 250 nm, within the natural variance of the diatoms.

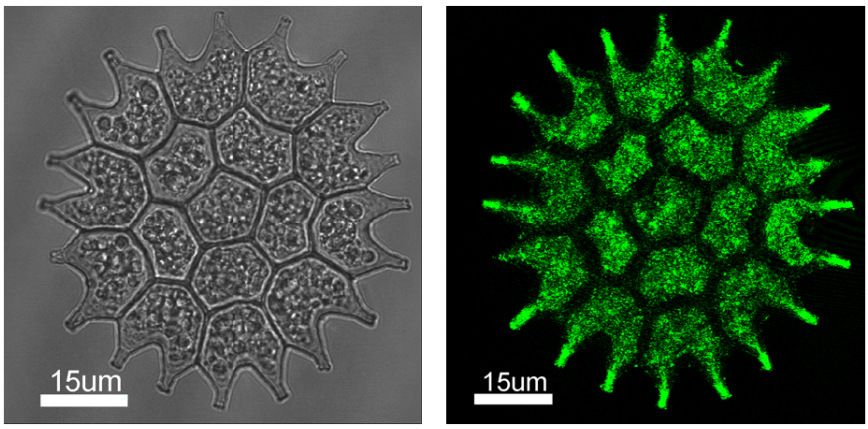

(a) (b)

Figure 6. (a) A bright field image of a *Pseudopediastrum* colony using an optical microscope. The crown structure and unit cells are well defined. (b) A slice of a bright field confocal image of the same *Pseudopediastrum* colony. The structure of the colony is best defined on the underside of the sample, before interference from other layers distorts the image.

The resolution of these images is currently comparable to the theoretical $(\delta x, \delta y, \delta z) = (140, 240, 140)$ nm achieved with the confocal system. However, our technique does not subject the sample to the focused laser light required in fluorescent confocal imaging, and does not suffer from a reduction in resolution caused by light scatter through the sample. While optical and confocal microscopy are diffraction-limited techniques, the resolution of our technique in x and y is limited by the probe's 250 nm radius of curvature and its residual Brownian motion (± 2 standard deviations $=$ 60 nm). The resolution in z is limited by the fine step size and Brownian motion, not tip size. Further reductions in the size of the probe could be achieved by identifying a biological probe with a sharper tip or by using some of the micro- or nanotools previously reported [24–26], therefore reducing tip convolution artefacts. Improvements in the trapping technique, such as position clamping the probe in 3D [23], could reduce the amplitude of the thermal motion of the tip. The technique itself is also easily parallelized. Using holographic optical tweezers [29], or other methods for rapidly generating numerous 3D-configurable optical traps, several probes could be scanned simultaneously. This would have the advantage of decreasing the imaging time and opens up the possibility of imaging a sample while external stimulation is occurring, for example, surface conformations could be imaged while a lipase is used to disrupt the cell membrane.

Conclusions

In summary, we have developed a form of SPM which utilizes holographically controlled probes whose trapping locations are largely removed from the sample–probe interaction area. The probes have the potential to be oriented, controlled and scanned in 3D, bypassing the planar scanning constraints of traditional SPM. This enables complex, highly curved samples to be scanned with a resolution comparable to confocal imaging. As the technique is not diffraction limited, there is scope for improvements in scanning resolution. Also, the technique

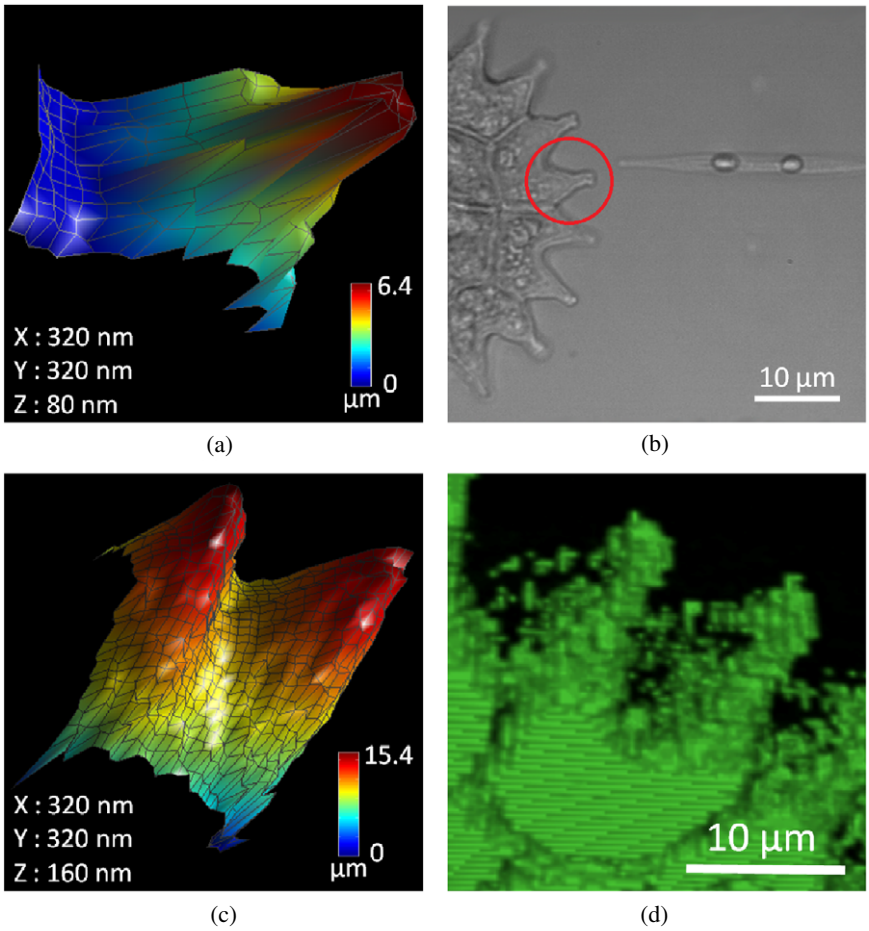

Figure 7. (a) The 3D surface image of the spike encircled in (b). (b) An optical microscope image showing an optically trapped diatom in the starting configuration (equivalent to State 1 in figure 2). The two optical traps are centred at each end of the elliptical handles. (c) The surface image following the scan of the side wall of a *Pseudopediastrum* unit cell. (d) A bright field confocal image of a similar sample, for comparison with (c).

imparts substantially less force than traditional contact SPM techniques. We have demonstrated this by imaging the side of a *Pseudopediastrum* unit cell which was not adhered to a surface. This technique could be used when certain limitations in existing technology are encountered and, in particular, for the investigation of significantly curved or soft cellular surfaces.

Acknowledgments

This work is funded by a Basic Technology Translation Grant through the Research Councils of the United Kingdom. MJM acknowledges a Royal Society Wolfson Merit Award. This work was carried out with the support of the Bristol Centre for Nanoscience and Quantum Information. We would also like to thank M Yallop, H Rosenkranz and D Fagan for culturing the original biological samples.

References

[1] Garcia R and Pérez R 2002 Dynamic atomic force microscopy methods *Surf. Sci. Rep.* **47** 197–301
[2] Santos N C and Castanho M A R B 2004 An overview of the biophysical applications of atomic force microscopy *Biophys. Chem.* **107** 133–49
[3] Hörber J K H and Miles M J 2003 Scanning probe evolution in biology *Science* **302** 1002–5
[4] Morita S, Abe M, Yokoyama K and Sugawara Y 2000 Defects and their charge imaging on semiconductor surfaces by noncontact atomic force microscopy and spectroscopy *J. Cryst. Growth* **210** 408–15
[5] Haberle W, Hörber J K H and Binnig G 1991 Force microscopy on living cells *5th Int. Conf. on Scanning Tunneling Microscopy/Spectroscopy (Boston, MA)* vol 9, AVS, pp 1210–3
[6] Schaer-Zammaretti P and Ubbink J 2003 Imaging of lactic acid bacteria with AFM—elasticity and adhesion maps and their relationship to biological and structural data *Ultramicroscopy* **97** 199–208
[7] Cross S E, Jin Y-S, Rao J and Gimzewski J K 2007 Nanomechanical analysis of cells from cancer patients *Nat. Nanotechnol.* **2** 780–3
[8] Hinterdorfer P, Baumgartner W, Gruber H J, Schilcher K and Schindler H 1996 Detection and localization of individual antibody–antigen recognition events by atomic force microscopy *Proc. Natl Acad. Sci. USA* **93** 3477–81
[9] Picco L M, Bozec L, Ulcinas A, Engledew D J, Antognozzi M, Horton M A and Miles M J 2007 Breaking the speed limit with atomic force microscopy *Nanotechnology* **18** 044030

[10] Ando T, Uchihashi T and Fukuma T 2008 High-speed atomic force microscopy for nano-visualization of dynamic biomolecular processes *Prog. Surf. Sci.* **83** 337–437
[11] Antognozzi M, Ulcinas A, Picco L, Simpson S H, Heard P J, Szczelkun M D, Brenner B and Miles M J 2008 A new detection system for extremely small vertically mounted cantilevers *Nanotechnology* **19** 384002
[12] Ashkin A, Dziedzic J M, Bjorkholm J E and Chu S 1986 Observation of a single-beam gradient force optical trap for dielectric particles *Opt. Lett.* **11** 288
[13] Florin E-L, Pralle A, Hörber J K H and Stelzer E H K 1997 Photonic force microscope based on optical tweezers and two-photon excitation for biological applications *J. Struct. Biol.* **119** 202–11
[14] Rohrbach A, Tischer C, Neumayer D, Florin E-L and Stelzer E H K 2004 Trapping and tracking a local probe with a photonic force microscope *Rev. Sci. Instrum.* **75** 2197–210
[15] Ghislain L P and Webb W W 1993 Scanning-force microscope based on an optical trap *Opt. Lett.* **18** 1678
[16] Friese M E J, Truscott A G, Rubinsztein-Dunlop H and Heckenberg N R 1999 Three-dimensional imaging with optical tweezers *Appl. Opt.* **38** 6597–603
[17] Nakayama Y, Pauzauskie P J, Radenovic A, Onorato R M, Saykally R J, Liphardt J and Yang P 2007 Tunable nanowire nonlinear optical probe *Nature* **447** 1098–101
[18] Gnecco E, Bennewitz R, Gyalog T, Loppacher Ch, Bammerlin M, Meyer E and Gntherodt H-J 2000 Velocity dependence of atomic friction *Phys. Rev. Lett.* **84** 1172
[19] Reicherter M, Haist T, Wagemann E U and Tiziani H J 1999 Optical particle trapping with computer-generated holograms written on a liquid-crystal display *Opt. Lett.* **24** 608–10
[20] Dufresne E R, Spalding G C, Dearing M T, Sheets S A and Grier D G 2001 Computer-generated holographic optical tweezer arrays *Rev. Sci. Instrum.* **72** 1810–6
[21] Gibson G, Carberry D M, Whyte G, Leach J, Courtial J, Jackson J C, Robert D J, Miles M J and Padgett M 2008 Holographic assembly workstation for optical manipulation *J. Opt. A: Pure Appl. Opt.* **10** 044009
[22] Gibson G M, Leach J, Keen S, Wright A J and Padgett M J 2008 Measuring the accuracy of particle position and force in optical tweezers using high-speed video microscopy *Opt. Express* **16** 14561–70
[23] Preece D, Bowman R, Linnenberger A, Gibson G, Serati S and Padgett M 2009 Increasing trap stiffness with position clamping in holographic optical tweezers *Opt. Express* **17** 22718–25
[24] Rodrigo P J, Gammelgaard L, Boggild P, Perch-Nielsen I and Glückstad J 2005 Actuation of microfabricated tools using multiple GPC-based counterpropagating-beam traps *Opt. Express* **13** 6899–904
[25] Ikin L, Carberry D M, Gibson G M, Padgett M J and Miles M J 2009 Assembly and force measurement with spm-like probes in holographic optical tweezers *New J. Phys.* **11** 023012
[26] Carberry D M *et al* 2010 Calibration of optically trapped nanotools *Nanotechnology* **21** 175501
[27] Glückstad J 2007 Manipulating microtools with nanofeatures using light in 3d real-time *iNANO Seminar (Arhus)*
[28] Simpson S H and Hanna S 2009 Thermal motion of a holographically trapped spm-like probe *Nanotechnology* **20** 395710
[29] Grier D G 2003 A revolution in optical manipulation *Nature* **424** 810–6